Heliyon 9 (2023) e17399

Contents lists available at ScienceDirect

Heliyon

journal homepage: www.cell.com/heliyon

Combining immunotherapy with high-dose radiation therapy (HDRT) significantly inhibits tumor growth in a syngeneic mouse model of high-risk neuroblastoma

Shuobo Boboila [a,2], Shunpei Okochi [b,2], Debarshi Banerjee [d,2], Sunjay Barton [a], Cherease Street [a], Ariela L. Zenilman [b], Qi Wang [a], Robyn D. Gartrell [c,d], Yvonne M. Saenger [d], David Welch [a], Cheng-Chia Wu [a], Angela Kadenhe-Chiweshe [a], Darrell J. Yamashiro [d,e,**,1], Eileen P. Connolly [a,*,1]

[a] *Department of Radiation Oncology, Columbia University Irving Medical Center, New York, NY 10032, USA*
[b] *Department of Surgery, Columbia University Irving Medical Center, New York, NY 10032, USA*
[c] *Department of Medicine, Columbia University Irving Medical Center, New York, NY 10032, USA*
[d] *Department of Pediatrics, Columbia University Irving Medical Center, New York, NY 10032, USA*
[e] *Department of Pathology, Columbia University Irving Medical Center, New York, NY 10032, USA*

ARTICLE INFO

Keywords:
Novel syngeneic mouse model
Neuroblastoma
High dose radiation therapy
Immunotherapy
MYCN-amplified neuroblastoma
Cancer therapeutics
Combination therapy

ABSTRACT

Purpose: The mortality in patients with *MYCN*-amplified high-risk neuroblastoma remains greater than 50% despite advances in multimodal therapy. Novel therapies are urgently needed that requires preclinical evaluation in appropriate mice models. Combinatorial treatment with high-dose radiotherapy (HDRT) and immunotherapy has emerged as an effective treatment option in a variety of cancers. Current models of neuroblastoma do not recapitulate the anatomic and immune environment in which multimodal therapies can be effectively tested, and there is a need for an appropriate syngeneic neuroblastoma mice model to study interaction of immunotherapy with host immune cells. Here, we develop a novel syngeneic mouse model of *MYCN*-amplified neuroblastoma and report the relevance and opportunities of this model to study radiotherapy and immunotherapy.

Materials and methods: A syngeneic allograft tumor model was developed using the murine neuroblastoma cell line 9464D derived a tumor from TH-MYCN transgenic mouse. Tumors were generated by transplanting 1 mm^3 portions of 9464D flank tumors into the left kidney of C57Bl/6 mice. We investigated the effect of combining HDRT with anti-PD1 antibody on tumor growth and tumor microenvironment. HDRT (8 Gy x 3) was delivered by the small animal radiation research platform (SARRP). Tumor growth was monitored by ultrasound. To assess the effect on immune cells tumors sections were co-imuunostained for six biomarkers using the Vectra multispectral imaging platform.

Results: Tumor growth was uniform and confined to the kidney in 100% of transplanted tumors. HDRT was largely restricted to the tumor region with minimal scattered out-of-field dose.

* Corresponding author. 622 W 168TH Street, CHONY North Bmst, Room 11, New York, NY, 10032, USA.)
** Corresponding author. 161 Fort Washington Ave, IP7, New York, NY, 10032, USA.)
E-mail addresses: dy39@cumc.columbia.edu (D.J. Yamashiro), epc2116@cumc.columbia.edu (E.P. Connolly).
[1] D. J. Yamashiro and E. P. Connolly contributed to this study.
[2] S. Boboila, S. Okochi and D. Banerjee contributed equally to this study.

https://doi.org/10.1016/j.heliyon.2023.e17399
Received 28 June 2022; Received in revised form 11 June 2023; Accepted 15 June 2023
Available online 19 June 2023

Combinatorial treatment with HDRT and PD-1 blockade significantly inhibited tumor growth and prolonged mice survival. We observed augmented T-lymphocyte infiltration, especially $CD3^+CD8^+$ lymphocytes, in tumors of mice which received combination treatment.
Conclusion: We have developed a novel syngeneic mouse model of MYCN amplified high-risk neuroblastoma. We have utilized this model to show that combining immunotherapy with HDRT inhibits tumor growth and prolongs mice survival.

1. Introduction

Neuroblastoma is the most common extracranial pediatric solid tumor with amplification of *MYCN* occurring in approximately 30% of cases [1,2]. M*YCN*-amplified neuroblastoma usually presents with aggressive high-risk metastatic disease, which despite multimodal intensive therapies often carries a poor prognosis [1–3]. Novel therapeutics approaches are urgently needed to treat high-risk neuroblastoma that will require preclinical evaluation of therapeutics in autologous preclinical neuroblastoma mice model.

Immunotherapy (IO), particularly immune checkpoint inhibitors (ICI) including programmed death receptor 1 (PD-1) and PD-ligand 1 (PD-L1) inhibitors, is an effective cancer treatment for several types of cancer (ref). In neuroblastoma, the addition of immunotherapy using the anti-disialoganglioside GD2 monoclonal antibody ch14.18 has demonstrated a significant improvement in survival for children with high-risk metastatic disease. However, ICI inhibitors, that show high efficacy in the treatment of adult cancers, demonstrate limited effectiveness in treating neuroblastoma patients, with minority of patients respond to single drug therapy. Therefore, multimodal therapeutic approaches currently being tested in clinical trials for high-risk neuroblastoma to improve effectiveness of IO and patient response.

One multimodal therapeutic approach that involves immunotherapy with high-dose radiotherapy (HDRT) has shown great promise in recent years in the treatment of a variety of cancers [4–6]. Recent studies have shown that HDRT inhibits tumor growth by direct killing of tumor cells and by the recruitment of the host immune response, which is exploited in immunotherapeutic approaches [4–6]. HDRT delivered as Stereotactic Body Radiation Therapy (SBRT), Stereotactic Radiosurgery (SRS) or Intraoperative Radiation Therapy (IORT) is increasingly being used in pediatric cancers [7–9]. HDRT improves the outcome for several high-risk neuroblastoma patients [10,11]. Given these advances there is great interest in immunotherapy in neuroblastoma, used alone or in combination with HDRT, to improve patient outcome.

This combined multimodal therapy in *MYCN*-amplified high risk neuroblastoma is largely untested in the preclinical setting due to the lack of a clinically-relevant syngeneic mouse model. One such current syngeneic mouse model, NXS2, is a hybrid cell line generated by fusion of Neuro-2a on A/J background and GD21 dorsal root ganglion cells in a C57Bl/6 background. Due to the differences in these two genetic backgrounds, NXS2 cells are immunogenic on both A/J and C57Bl/6 backgrounds and therefore are not suitable for immunotherapeutic testing [12]. Another syngeneic mouse model, Neuro-2a, does not express GD2 and other key target antigens [13]. Weiss et al. developed a transgenic *TH-MYCN* murine neuroblastoma model in which *MYCN* expression is driven by a rat tyrosine hydroxylase (*TH*) promoter and tumors closely resemble high-risk human neuroblastoma [14]. This model provides faithful recapitulation of neuroblastoma development in mice, but tumor development occurs over a significantly more prolonged period and tumor incidence in heterozygous mice is low and unpredictable [15,16].

Here, we developed a neuroblastoma syngeneic mouse model by transplanting the TH-MYCN-derived neuroblastoma cell line 9464D into C57Bl/6 mice, and utilized this model to test efficacy of IO and HDRT, single or in combination therapy, in preclinical high-risk neuroblastoma. We demonstrated that the combination of HDRT and PD-1 blockade inhibits neuroblastoma tumor growth and stimulates immune response by enhancing $CD8^+$ T lymphocyte infiltration.

2. Materials and methods

2.1. Cell culture

The 9464D cell line, derived from a TH-MYCN transgenic neuroblastoma mouse, was obtained as a gift from Dr. Crystal Mackall at the National Institute of Health (NIH). Cells were cultured in DMEM with 10% FBS and 1% non-essential amino acids. The cell line was authenticated by short tandem repeat profiling (ATCC).

2.2. Syngeneic transplantation tumor model

All procedures performed were approved by The Institutional Animal Care and Use Committee (IACUC) of Columbia University (protocol approval number AABQ7586). 7 week old female C57BL/6 mice were purchased from Charles River. 1×10^6 9464D cells were subcutaneously injected into the right flank of "donor" mice. Tumor growth was monitored by caliper measurement. Tumors were explanted when they reached 1 cm^3, washed in sterile saline, divided into 1 mm^3 portions and placed in DMEM culture medium in preparation for implantation. Simultaneously, "recipient" mice were prepped and draped in standard surgical fashion to expose the left flank. Animals were anesthetized with an intraperitoneal injection of 80–100 mg/kg ketamine and 5–10 mg/kg xylazine, and 0.5 mg/kg buprenorphine given for pain management. A 5 mm incision was made in the left flank, and the kidney was mobilized and exposed. A 1 mm incision was made in the renal capsule away from the hilum and the 1 cm^3 portion of tumor implanted into the kidney

parenchyma. Hemostasis was achieved with direct pressure. The renal capsule was closed with a monofilament nonabsorbable suture, peritoneum and fascia closed with absorbable polyfilament suture and skin approximated with surgical clips.

2.3. Ultrasound imaging

Growth of the intrarenal transplanted tumors was monitored by ultrasound. Mice were anesthetized with inhaled isoflurane anesthetic. 100 μl of sterile saline solution was then intraperitoneally injected to facilitate separation of bowel and solid organs. Mice were imaged by ultrasound using the Visualsonics VEVO 2100 Ultrasound Imaging System [16,17].

2.4. Syngeneic tumor treatment

Once the tumor reached a size of 0.5 cm^3, as measured by on ultrasound, the mice were randomly enrolled (day 0) into one of four treatment groups: (i) placebo, (ii) anti-PD1 antibody, (iii) 8Gy x 3 HDRT and (iv) HDRT + anti-PD1. Mice received 200 μg of anti-PD1 antibody (CD279, BioX Cell, clone 29F.1A12) [18–20] via intraperitoneal injections on day 0, 3 and 6 post-enrollment. HDRT was given on day 3, 5 and 7 in 8Gy fractions. Half of the mice from each group were sacrificed on day 9 post-enrollment (early) and the other half were sacrificed when their tumor size reached 1.5 cm^3 (late) as measured by ultrasound.

2.5. Small animal radiation research platform (SARRP)

HDRT was delivered using the Small Animal Radiation Research Platform (SARRP; Xstrahl, Camberely, UK). Mice were anesthetized with 1% isoflurane and immobilized on the SARRP's robotically-positioned treatment bed and iohexol contrast (300mgI/mL, GE Healthcare) was administered via intraorbital injection. Images were transferred to MuriPlan software, the intrarenal tumor was contoured and the treatment isocenter was placed in the center of tumor volume. All treatments were conducted with 220 kV photons with 0.15 mm copper filtration. 24 Gy was delivered in 3 fractions at 8Gy per fraction on days 3, 5 and 7 after enrollment, using two 170° arcs with an attached 1 x 1-mm collimator.

2.6. Mouse-like phantom analysis

To assess for radiation delivery accuracy, mouse-like phantom analysis were performed, as previously described in Welch et al. [21,22]. One mouse like phantom is in the sagittal arrangement, and a second is in the coronal arrangement. Radiochromic film, EBT3 (Ashland Advanced Materials, Niagara Falls, NY), was placed at the center of the tumor region in both the coronal and the sagittal phantoms. After calibration of the radiochromic films, absolute dose distributions of irradiated films were analyzed based on the optical density distribution and H-D curve. Doses of 8 Gy were delivered to both the sagittal and the axial phantom, and radiochromic films were analyzed. The radiochromic film was scanned within 12 h of delivery of radiation using an Epson Expression (Long Beach, CA) 11000XL flatbed scanner with professional mode, positive film type, transparency mode, and no color correction settings. The irradiated films were scanned at 300dpi resolution.

2.7. Quantitative multispectral immunofluorescence (qmIF)

Full-section 5-μm slides of formalin fixed paraffin embedded tumor, kidney and spleen tissue specimens were stained using Opal multiplex 6-plex kits, following the manufacturer's protocol (PerkinElmer). Briefly, tissue slides were baked for 2 h at 60 °C and then deparaffinized in xylene and rehydrated with a series of graded ethanol solutions. Antigen retrieval was performed using microwave treatment for 20 min in antigen retrieval solution pH6 (AR6). After the serial incubation with the following primary antibodies (Supplementary Table 1): CD3 (Spring Biosciences), CD8 (eBiosciences), CD4 (eBiosciences), FOXP3 (eBiosciences), endomucin (Santa Cruz Biotechnology), for 1 h at room temperature, sections were labeled with the anti-rabbit/mouse Polymeric Horseradish Peroxidase (Opal IHC Detection Kit, Akoya Biosciences) for 10 min at room temperature. Subsequently, tissue sections were incubated with TSA-conjugated fluorophores (Opal 540 for CD3, Opal 620 for CD4, Opal 570 for CD8, Opal 690 for endomucin, and Opal 520 for FOXP3; PerkinElmer) for 10 min. The signal for antibody was visualized by their corresponding Opal Fluorophore (Akoya Biosciences) after a 10-min incubation. And a heat-mediated stripping step was inserted between each antibody staining round. Finally, all slides were counterstained with DAPI (Abcam) for 5 min, then mounted with an anti-fade mounting medium (Abcam) and stored at 4 °C before imaging.

Controls slides labeled with individual antibodies and an unstained slide were used to normalize fluorescence intensity. The multiplex IF slides was scanned at 10 × with the Vectra 3 Automated Quantitative Pathology Imaging System (PerkinElmer) using spleen and kidney as controls to calibrate the spectral image protocol (Fig. S2). Specimens were sampled from five individual fields (1338 μm × 1000 μm) randomly in the intratumoral compartment and spleen compartment by using the Phenochart™ whole slide contextual viewer 1.0.4 (PerkinElmer) software to scan at high resolution (× 20) in order to capture high-powered field (Fig. S2). At least 5 randomly chosen fields per tumor were analyzed for quantification. Multispectral images were decomposed into their various components by spectral unmixing using a digital spectral library consisting of spectral profiles of each of the fluorophores using Inform (v2.4.1, PerkinElmer) software. Then tissue segmentation (trainable to 98% accuracy) and cell segmentation were performed (nuclear compartment —DAPI, FOXP3; cytoplasmic-endomucin, membrane—CD3, CD4, CD8), and cells were phenotyped on the basis of expression of one or multiple markers. Entire cell mean fluorescent units were extracted for each marker and normalized as a percentile

of maximum and minimum fluorescence across all cells in all images. Afterwards, cells were phenotyped for marker expression in separate software designed in RStudio (version 0.99.896; https://github.com/thmshrt/transform_essential) [23,24]. In this software, images were combined and analyzed to concatenate variables and determine density of distinct phenotypes. $CD3^+$ T cells, $CD3^+CD8^+$ T cells, $CD3^+CD4^+$ T cells and $CD3^+CD4$+FOXP3+ Treg cell number per high powered field was quantified.

2.8. Statistical analysis

Statistical analysis for the experiments was performed using Prism software (GraphPad) [23]. Normal data was analyzed by unpaired *t*-test or ANOVA with post-hoc analysis by Tukey's Multiple Comparison test. Graphs represent mean and standard deviation in all cases. The level of significance was considered $p \leq 0.05$.

3. Results

3.1. A reproducible syngeneic neuroblastoma mouse model

The 9464D cell line is derived from spontaneous neuroblastoma tumor in TH-MYCN mouse in a C57BL/6 background [14]. TH-MYCN transgenic mice spontaneously develop abdominal neuroblastoma tumor that genetically and histologically resemble human neuroblastoma [14,16]. 9464D cells contain human *MYCN* and expresses human MYCN transcript (data not shown). 9464D cells also express GD2 and other immune markers. In order to develop syngeneic tumor in mice we performed initial experiments where cells were directly injected into adrenal gland and kidney. The majority of neuroblastoma in children arise from the adrenal gland, with a minority of cases in extra-adrenal sites [3,24]. Invasion of neuroblastoma into the renal parenchyma also occurs in 20% of cases [25,26]. In order to develop syngeneic murine neuroblastoma tumors, we initially injected 9464D neuroblastoma cells directly into adrenal gland and kidney. However due to the highly aggressive nature of the 9464D cells the resultant tumors were not confined within adrenal gland or kidney capsule and extensive seeding throughout the peritoneal cavity was observed (data not shown). To address these limitations, we generated flank tumors by subcutaneous injection of tumor cells, explanted them, divided them into ~1 mm^3 portions (Fig. 1A), and implanted one portion into renal parenchyma of C57BL/6 mice (Fig. 1A). Tumor growth was monitored by ultrasound (Fig. 1B). We observed 100% tumor uptake (15/15) with tumor confined to the kidney in all mice (Fig. 1C). In this cohort of

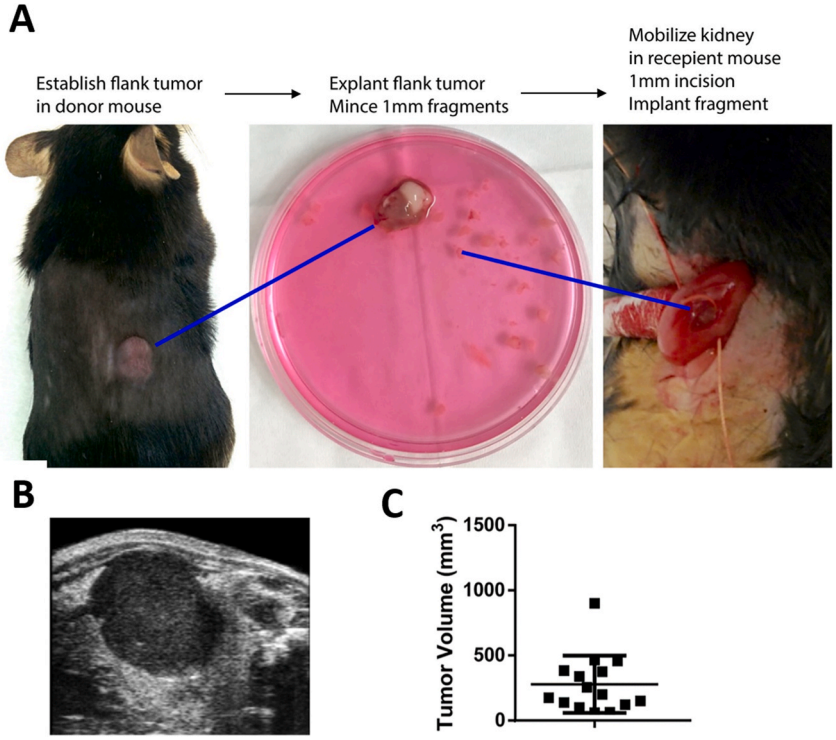

Fig. 1. Intrarenal syngeneic transplantation mouse model of neuroblastoma. (A) A flow diagram shows the generation of mouse model. 9464D cells were initially injected into the flank of C57BL/6 mice. Once the flank tumor size reached 1 cm^3 , ' as measured by ultrasound, it was explanted, divided into 1 mm^3portions and placed in DMEM culture medium. White arrows designate the portions of explanted tumor. Simultaneous to the tumor explant, recipient mice were prepared for tumor implant. One piece of the explanted tumor was surgically implanted within the renal parenchyma of a recipient C57BL/6 mouse (n = 15). White arrow points to the implantation site within the kidney. **(C)** Representative ultrasound image of a tumor. **(D)** Tumor volumes measured by ultrasound on day 13 post implantation (n = 15).

15 mice, on day 13 post implantation, tumor volumes were 280 mm^3 on average, with a standard deviation of 220 mm^3.

3.2. HDRT is delivered accurately to the tumor region

High dose radiation (HDRT) was delivered using the Small Animal Radiation Research Platform (SARRP), which mimics SBRT radiation treatment in patients [27]. Mice were anesthetized and iohexol contrast agent was administered. Computed tomographic (CT) scans were taken from coronal, sagittal, and axial planes to locate the tumor. We found that CT scan images taken within minutes post administration of iohexol contrast agent allowed clear delineation of the tumor within the renal parenchyma (Fig. 2A). Using tumor volume contoured on the CT scan images 8 Gy radiation was delivered using two 170° arcs with an attached 1 x 1-mm collimator. The isodose lines generated with MuriPlan showed that HDRT was delivered within a confined field, with little penumbra to other organs (Fig. 2B).

To assess the accuracy of radiation targeting and quantify the actual dose delivered to the tumor, mouse like phantoms with radiochromic film were used, according to the design previously described by Welch and colleagues [21]. Single-arc 8 Gy in the coronal orientation was planned and delivered with the same parameters used for the live animals (Fig. 2C). Isodose lines were created in MATLAB based on the inverse intensity projected on the radiochromic film. The isodose lines were overlaid onto a scanned image of the radiochromic film with the phantom, and the radiochromic film was further analyzed using H-D curves generated in our department (Fig. 2D). Film analysis showed the phantom film received a Dmax of 849.7 cGy, and insignificant amounts of overdose

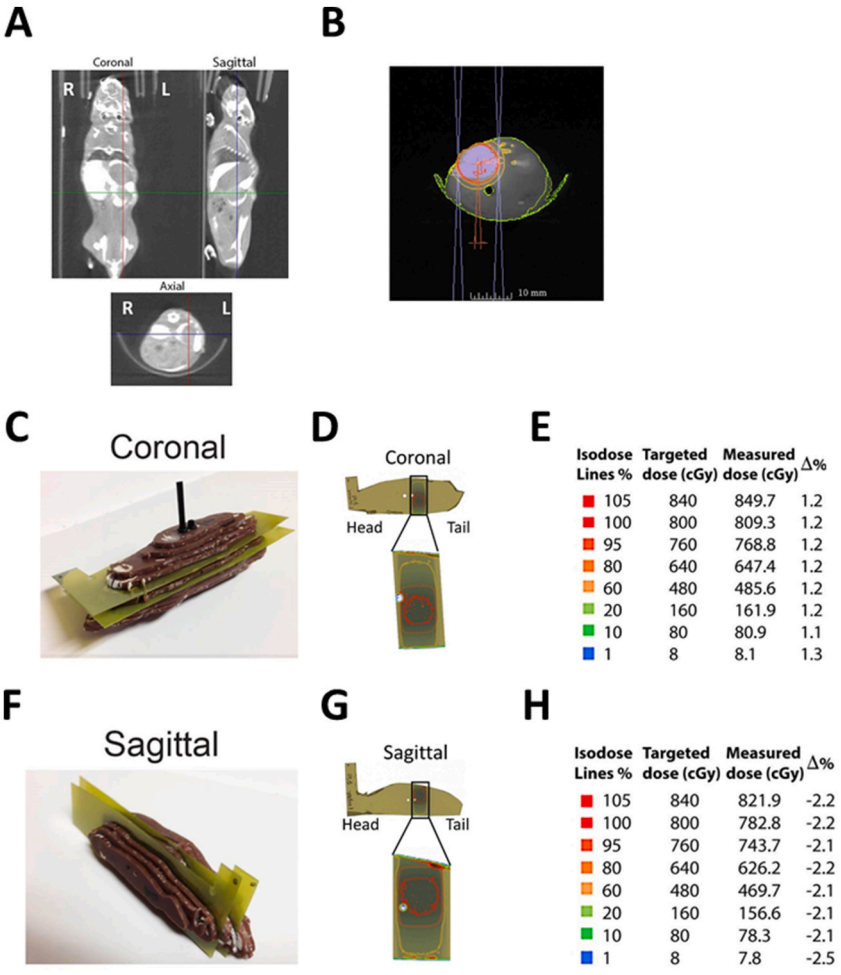

Isodose Lines %	Targeted dose (cGy)	Measured dose (cGy)	Δ%
105	840	849.7	1.2
100	800	809.3	1.2
95	760	768.8	1.2
80	640	647.4	1.2
60	480	485.6	1.2
20	160	161.9	1.2
10	80	80.9	1.1
1	8	8.1	1.3

Isodose Lines %	Targeted dose (cGy)	Measured dose (cGy)	Δ%
105	840	821.9	-2.2
100	800	782.8	-2.2
95	760	743.7	-2.1
80	640	626.2	-2.2
60	480	469.7	-2.1
20	160	156.6	-2.1
10	80	78.3	-2.1
1	8	7.8	-2.5

Fig. 2. 3D computed tomography (CT) scan based radiation treatment planning. (A) Two 170°arcs were designed to deliver 8Gy radiation, using a 1 cm × 1 cm collimator. Images were taken from the coronal plane, the sagittal plane, and the axial plane. **(B)** Isodose lines from an axial plan. Computed tomographic simulation was performed, and a representative mouse CT imaging scan was used to contour the gross tumor volume (GTV). Two 170° arcs were created targeting the GTV. **(C)** Phantom mouse construct from the coronal plane view. **(D)** Radiochromic film after coronal radiation delivery. Isodose lines were created based on the inverse intensity projected on the phantom based radiochromic films. **(E)** Measured dosage on the coronal radiochromic film. **(F)** Phantom mouse construct from the sagittal plane view. **(G)** Radiochromic film after sagittal radiation delivery. **(H)** Measured dosage on the sagittal radiochromic film.

(1.2% on average) (Fig. 2E). We performed similar analysis with single-arc 8Gy radiation delivered in the sagittal orientation (Fig. 2F and G). We obtained a Dmax of 821.9 cGy, and an average of 2.2% under dose (Fig. 2H). To determine the out-of-field dosage, we analyzed the radiation amount on the phantom films 10 mm away from the isodose center in the coronal orientation, and 14 mm away from the isodose center in the sagittal orientation. We found a Dmax of 212.6 cGy in the coronal orientation, and a Dmax of 161.5 cGy in the sagittal orientation (Fig. S1). More than a four-fold decrease in radiation dosage was measured on the off iso-center films, indicating that there was little scattered radiation delivered outside of the tumor region. Together, our analysis confirms that HDRT can be delivered accurately to the target tumor region only.

3.3. Combination of HDRT and PD-1 blockade inhibits neuroblastoma tumor growth

Several preclinical studies on adult and children cancers have shown that HDRT in combination with checkpoint PD-1/PD-L1 inhibitors, showed greater anti-tumor efficacy than either therapy alone [6,28,29]. However, the effect of this combination therapy has been largely untested in neuroblastoma. Neuroblastoma cells have been shown to express PD-L1 [30]. Additionally, HDRT has been demonstrated to be efficacious in the treatment of high-risk neuroblastoma [10,31]. Therefore, we decided to use our model to determine whether combining HDRT with anti-PD1 treatment would have greater efficacy in inhibiting tumor growth. The treatment schema is illustrated in Fig. 3A. Mice, bearing 9464D tumors, were randomly enrolled, on day 0, into 4 treatment groups; (i) placebo, (ii) anti-PD1 antibody, (iii) HDRT (8 Gy x 3) and (iv) HDRT + anti-PD1 with same dose regimen (Fig. 3A). Mice were treated with

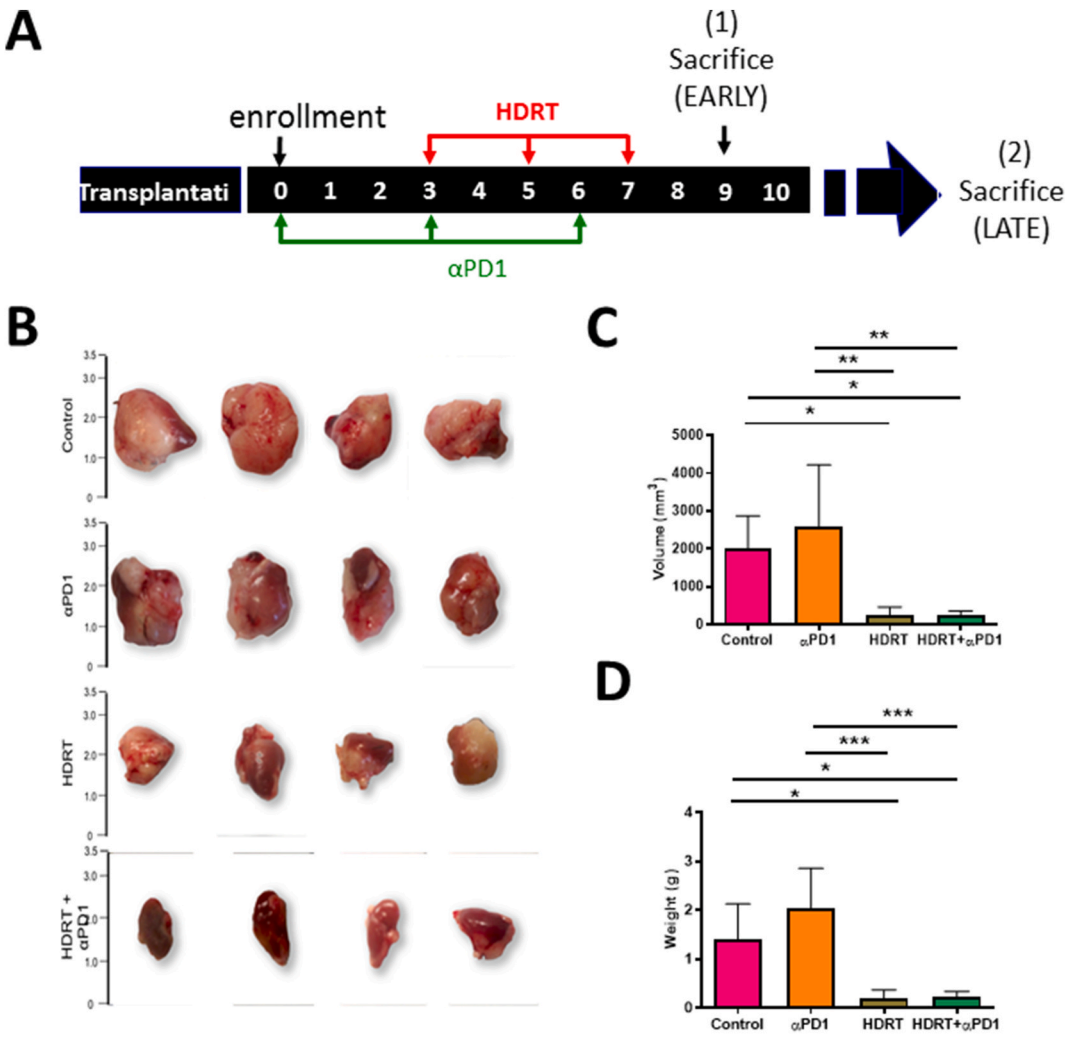

Fig. 3. HDRT inhibits tumor growth at early time point. (A) Schema of anti-PD1 antibody and radiation treatments in 9464D syngeneic intrarenal tumors. Mice were enrolled on day 0. Mice were treated with anti-PD1 antibody on day 0, 3, 6 and 8 Gy fractions on day 3, 5 and 7 post-enrollment. Mice were subjected to early sacrifice (early time point) on day 9 and late sacrifice at 1.5 cm^3 tumor size. **(B)** Representative gross images of tumors for each treatment group at early sacrifice time point. Mice were sacrificed on Day 9 as described in A. **(C)** Tumor volume at early time point (Day 9). Tumor volume was measured by ultrasound. **(D)** Tumor weight at early time point (Day 9).

anti-PD1 antibody on day 0, 3, 6 post-enrollment and 8 Gy dose of HDRT on day 3, 5, 7. Half of the mice from each group were sacrificed at early time point on day 9 post-enrollment, which was 2 days after the last fraction or 3 days after the last treatment of anti-PD-1 antibody (Fig. 3A). We observed that HDRT significantly reduced tumor growth of 9464D tumors (Fig. 3B) as depicted from tumor volume (Fig. 3C) and tumor weight measurement (Fig. 3D). Anti-PD1 had no effect on either tumor volume or tumor weight at the early time point and anti-PD1 +HDRT treatment, comparing with HDRT treatment alone, showed no changes on tumor growth (Fig. 3B–D).

The other half of the mice were monitored for tumor growth by ultrasound and were sacrificed, at late time point, when tumor volume reached 1.5 cm^3. As shown in Fig. 4A the control tumors showed rapid growth and PD-1inhibtion had no effect on tumor growth over time. We observed significant inhibition of 9464D tumor growth when combining HDR with anti-PD1 treatments. Kaplan-Meier survival analysis further showed that HDRT prolonged the survival of mice increasing median survival by 16 days (Fig. 4B; 27 vs. 11 days, HDRT vs. control 0 Gy, respectively). Combining HDRT with PD1 inhibition further prolonged mice survival with median survival of 52 days observed (Fig. 4B). Together, these results demonstrate that anti-PD-1 combined with HDRT showed greater inhibition of tumor growth than HDRT alone.

3.4. *Combination of HDRT and PD-1 blockade promotes $CD8^+$ T-lymphocyte infiltration 48 h post treatment*

Radiotherapy can change immune landscape by increasing infiltration of T lymphocytes into the microenvironment [6,28,29].

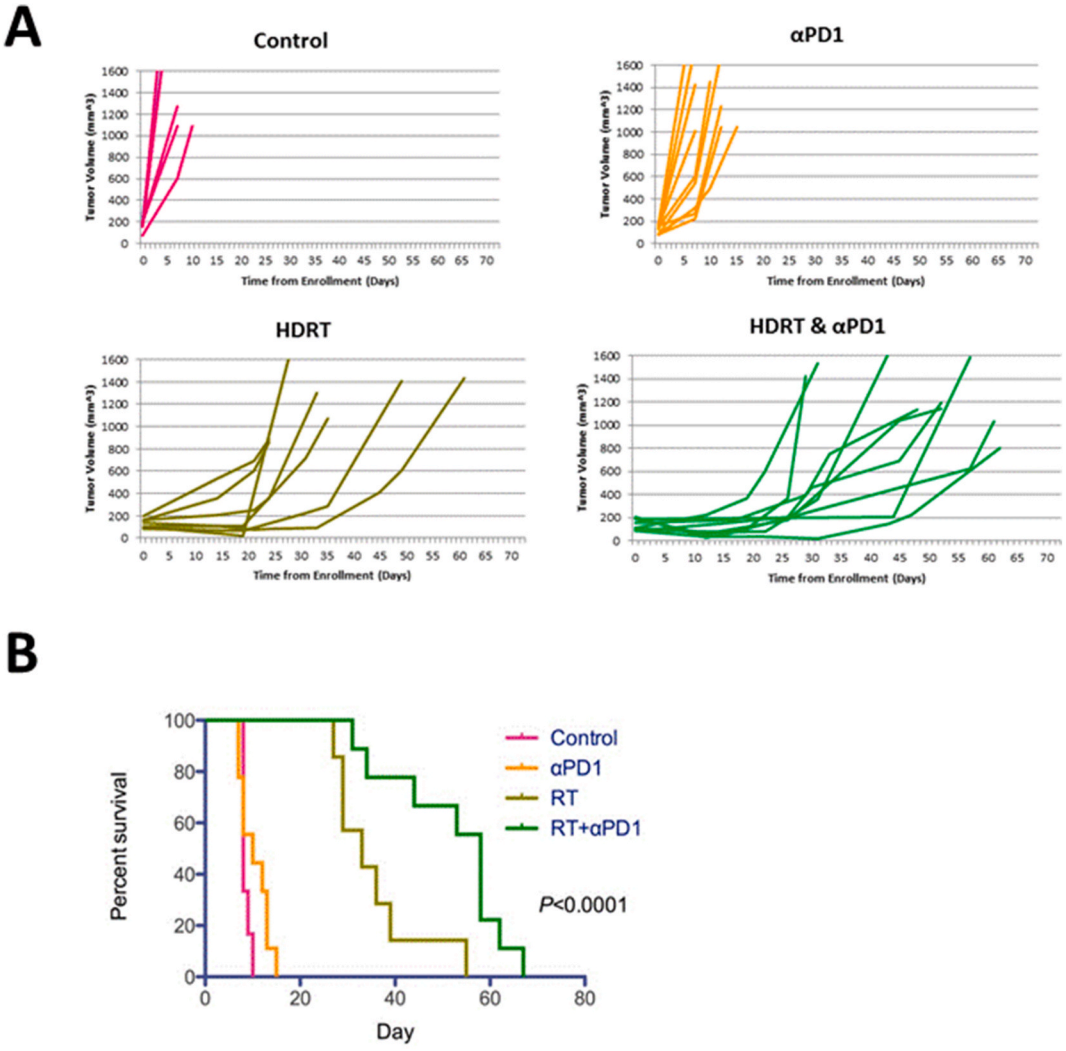

Fig. 4. Combination of anti-PD-1 blockade and HDRT inhibits 9464D tumor growth. (A) Tumor growth with time for 4 treatment groups. Tumor volume was measured by ultrasound. Mice were enrolled on day 0. Mice were treated with anti-PD1 antibody on day 0, 3, 6 and 8 Gy fractions on day 3, 5 and 7 post-enrollment. **(B)** Kaplan–Meier analysis of mice, bearing 9464D tumors, from 4 treatment groups. Survival was defined as the day when tumor volume reached 1.5 cm^3 and mouse was sacrificed.

Next, we characterized immune microenvironment, using quantitative multiplex fluorescence technology [32], by coimmunostaining for CD3 (lymphocyte marker), CD4 (T-helper marker), CD8 (cytotoxic T-lymphocyte marker), FOXP3 (T regulatory lymphocyte marker), endomucin (vascular marker), and DAPI (nuclear marker). We observed little $CD3^+$ lymphocyte infiltration in the control, untreated tumors (Fig. 5A). In contrast, treatment with either anti-PD-1 antibody, or HDRT increased the intra-tumor $CD3^+$ lymphocyte infiltration, at early time point, with the highest number of $CD3^+$ lymphocytes observed in the tumors of mice which received combination treatment (Fig. 5A). Quantification of cell number per high-powered field showed a ~25 fold and ~30 fold increases of $CD3^+$ lymphocytes in tumor treated with anti-PD1 antibody and HDRT, respectively, compared to control tumors at early time point (Fig. 5B). Consistent with $CD3^+$ cells, increased of $CD3^+CD8^+$ T-cells were detected in HDRT + anti-PD1 tumors, at early time point, compared to control tumors (Fig. 5C). There was no change in the numbers of $CD3^+CD4^+$ T-cells (Fig. 5D) and $CD3^+CD4$+FOXP3+ T-reg cells (Fig. 5D) observed in combination treatment group. Therefore, our data indicates that HDRT and PD-1 blockade combined-treatment promotes anti-tumor immunostimulatory immune response by increasing $CD8^+$ T-lymphocyte infiltration as early as 48 h post irradiation.

We also characterized the immune response at late time point (Fig. 6A). We observed a 1.5 fold increase of $CD3^+$ cells (Fig. 6B), 2 fold increase of $CD3^+CD8^+$ T cells (Fig. 6C), 3 fold increase $CD3^+CD4^+$ T cells (Fig. 6D) in HDRT + anti-PD1 treated tumors compared to only HDRT. No significant difference in the number of immunosuppressive $CD3^+CD4$+FOXP3+ T-reg cells was detected between the two groups (Fig. 6E). Therefore, our data showed that combination of HDRT and anti-PD-1 immunotherapy results in a persistent, long-term augmentation in the anti-tumor immune response.

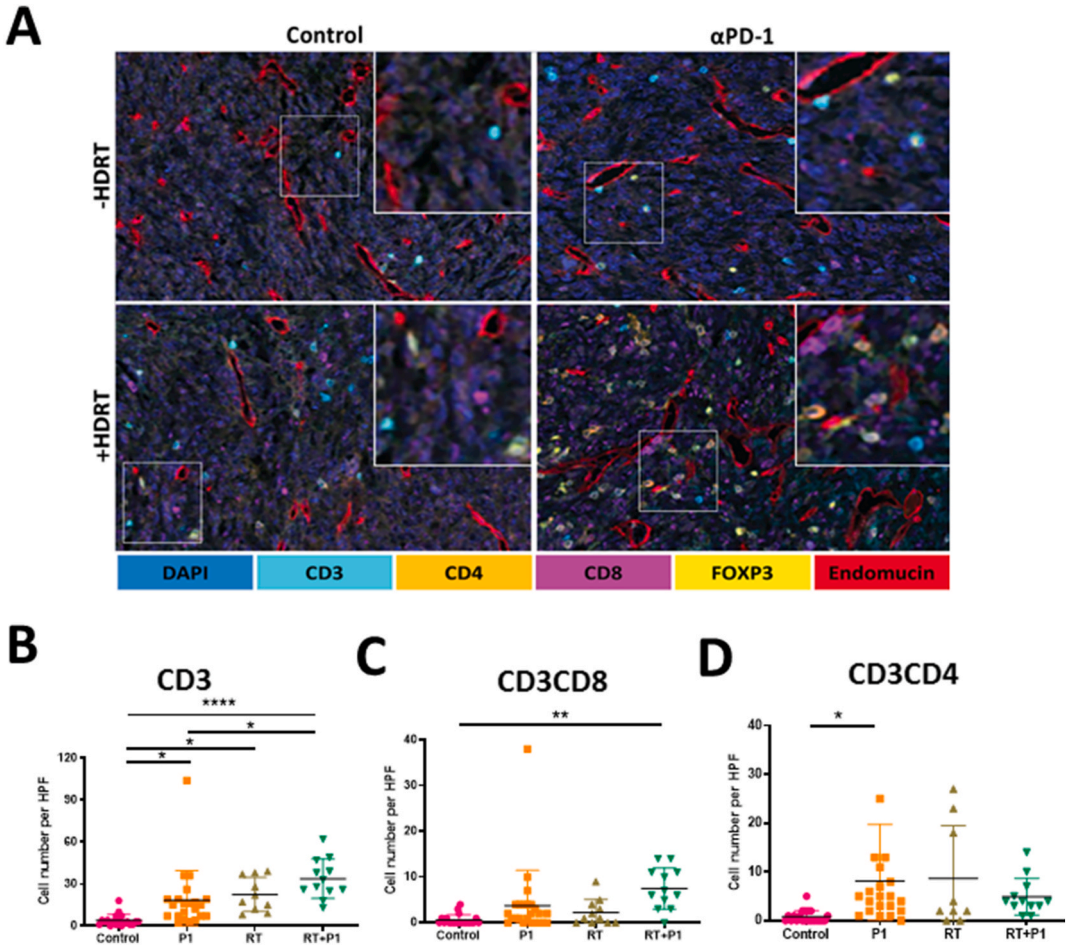

Fig. 5. Combining HDRT with PD-1 inhibition increased cytotoxic $CD3^+CD8^+$ T-cell infiltration at early time point. (A) Representative images of quantitative multiplex immunofluorescence staining for DAPI (blue), CD3(cyan), CD4 (orange), CD8 (magneta), FOXP3 (yellow) and endomucin (red) at early time point. Mice were sacrificed at day 9 of the treatment regimen, tumors were formalin fixed and stained using Opal multiplex 6-plex kits with antibodies for CD3 (cyan), CD4 (orange), CD8 (Magenta), FOXP3 (yellow) and endomucin (red). DAPI is used as counterstain. Quantification of cell number per high-powered field for **(B)** $CD3^+$ T cells, **(C)** $CD3^+CD8^+$ T cells, **(D)** $CD3^+CD4^+$ T cells and **(E)** $CD3^+CD4$+FOXP3+ Treg cell. Mean ± SD. *, $p < 0.05$; **, $p < 0.01$; ****, $p < 0.0001$. For details of staining and quantification processes please see Material and Methods. (For interpretation of the references to color in this figure legend, the reader is referred to the Web version of this article.)

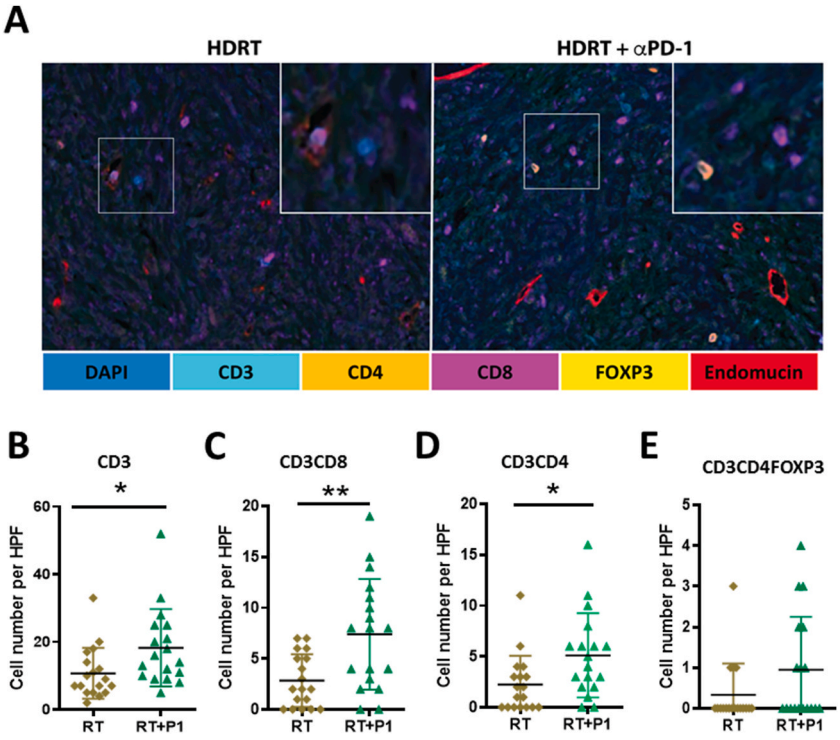

Fig. 6. Elevated numbers of cytotoxic T-cells and T-helper cells in the combination group at late time point. A) Quantitative multiplex immunofluorescence images of T cell population in 9464D tumors. Tumors were coimuunostained for 6 markers: DAPI, blue; CD3, cyan; CD4, orange; CD8, magenta; FOXP3, yellow; Endomucin, red. Mice were sacrificed at 1.5cm3 tumor size and tumors were subjected to multiplex immunofluorescence staining (details of staining in Material and Methods). Quantification of cell number per high-powered field for **(B)** $CD3^+$ T cells, **(C)** $CD3^+CD8^+$ T cells, **(D)** $CD3^+CD4^+$ T cells and **(E)** $CD3^+CD4$+FOXP3+ Treg cells. Mean ± SD. *, $p < 0.05$; **, $p < 0.01$. Mice were subjected to early sacrifice (early time point) on day 9 and late sacrifice at 1.5 cm^3 tumor size. (For interpretation of the references to color in this figure legend, the reader is referred to the Web version of this article.)

4. Discussion

Enhancement of the anti-tumor immune response by blocking immune checkpoint pathways and HDRT has emerged as an effective and complementary approach to the therapeutic mainstays of surgery, chemotherapy, and radiation in neuroblastoma treatment. However, existing neuroblastoma mice models are not appropriate to study interaction of radiation with host immune microenvironment. Current mice models of neuroblastoma research includes human xenograft, transgenic and syngeneic animal models [33,34]. Xenograft murine models, where human cells are injected to mice to develop human tumors, use athymic nude mice that lack T cells [35]. Patient-derived xenograft (PDX) models of neuroblastoma involves incorporation of human patient tumor fragments via subcutaneous or orthotopic injection into mice. These models also use immunocompromised mice that lack intact immune systems [33]. Therefore, these two models are inadequate to study the effect of drugs on fully intact immune microenvironment [16,36].

Syngeneic mice models have functional intact immune system. Two most common syngeneic mice models of neuroblastoma research and drug efficacy studies are Neuro-2a cells and NXS2 mice models. However, these models are not appropriate to study immune response in high-risk neuroblastoma. Neuro-2a cells are from mice in A/J background and devoid of GD2 and certain immune markers [13]. NSX2 is a hybrid cell line generated by fusing Neuro-2a on A/J background and GD2+ dorsal root ganglion cells on C57Bl/6 background [12]. Therefore, these cells are not fully autologous on A/J or C57Bl/6 background. Transgenic murine models are devoid of any such inadequacies. Transgenic murine models overcome some of the disadvantages associated with syngeneic models. TH-MYCN transgenic mice generates spontaneous tumor which contains human MYCN amplification and resembles high risk MYCN amplified human tumors with genetics and histological relevance. However, tumor incidence in the heterozygous mice is low and unpredictable and tumor development is prolonged [14,16]. Here, we develop an autologous human *MYCN* amplified neuroblastoma mice model generated from transplantable *MYCN* transgenic cell line 9464D in C57Bl/6 mice. With tumor uptake rate of 100% and uniform sizes of tumor confined within the kidney and predictable growth rates, this model is highly reproducible and reliable.

Neuroblastoma most commonly originates from cells within adrenal gland, however there is invasion into the kidney in up to 20% of reported cases [25]. Our lab has previously developed an intrarenal xenograft model of human neuroblastoma for preclinical studies by injecting human tumor cells directly into the kidney [23,37–39]. This model has subsequently been utilized by others in multiple publications in the neuroblastoma research [36]. We initially injected 9464D cells directly into the orthotopic organs. However due to

the highly aggressive nature of the 9464D cells, tumors were not confined into the kidney with multiple tumor deposits observed throughout the peritoneal cavity despite optimal technique, which made the tumors impossible to target by HDRT. We therefore followed the current approach by implanting a 1 mm^3 portion of subcutaneous tumor from "donor" mice to the kidney of "recipient" mice.

We delivered HDRT via the small animal radiation research platform (SARRP-200, Xstrahl). This state-of-the-art conformal irradiator features x-ray tomographic guidance which allows for conformal irradiation of targeted organs and locations. We showed that we could clearly delineate the tumor region on CT scan images and we were able to set HDRT to target a confined region within the abdomen of the animal. Phantom film analysis showed that 8Gy of radiation was accurately delivered to the tumor region, with less than 3% variation and minimal out-of-field spread to other organs/locations within the mouse. All mice survived after radiation treatment and we observed no late GI toxicity due to radiation. Overall, we demonstrated that we are able to accurately deliver highly conformal HDRT to a mouse abdominal tumor with minimal toxicity, in a manner that mimics stereotactic body radiation treatment in patients. We used multiplex immunofluorescence staining to characterize immune cells. Multiplex staining allowed us to co-immunostain up to six markers to simultaneously identify multiple cell types in a single tissue section and characterize their spatial distribution within the tumor.

We utilized our model to assess the effect of combining radiotherapy with anti-PD1 blockade. Radiotherapy can reprogram tumor microenvironment to exert anti-tumor immune response that can be exploited with immunotherapy to improve treatment efficacy. There is a great interest to investigate the effect of this combined-modality treatment on several adult and children tumors in pre-clinical studies and translate the findings in clinical trials. Anti-PD-1 agents inhibit the interaction between PD-1 and its ligand PD-L1, and thus activate the cytotoxic T-cells immune response [26]. In a preclinical model of melanoma and renal cell cancer, the combination of anti-PD-1 therapy and HDRT led to tumor growth inhibition [28]. This effect was attributed to immune-mediated killing of tumor cells by greater exposure of tumor antigens to cytotoxic T cells. It was recently demonstrated that PD-L1 is expressed by neuroblastoma cells [27] suggesting that PD-1 blockade may be a useful adjuvant in treatment of the disease. Our study shows that PD1 blockade alone has no effect on tumor growth in the 9464D tumor model. However, combining HDRT with PD1 blockade exhibits greater efficacy in inhibiting 9464D tumor growth and prolonging mice survival than HDRT treatment alone. The inhibition of tumor growth was associated with increased cytotoxic T lymphocyte infiltration throughout the time course of tumor development. These suggest combination of radiotherapy and immunotherapy has potential to improve treatment outcome in clinic.

One limitation of our study is that it does not explore the effect of HDRT and immunotherapy on immune cells other that T cells. Like T cells, a variety other immune cells such as macrophages, myeloid-derived suppressor cells, dendritic cells, natural killer cells, and neutrophils contribute to tumor progression. Macrophages are important immune cells that are directly implicated in the tumor control in response to radiation. HDRT attracts immunostimulatory anti-tumor M1-type tissue-associated macrophages (TAM) [40, 41]. HDRT has also been shown to attract immunosuppressive pro-tumorigenic M2-type TAM that contributes to minimizing HDRT effects and tumor regrowth [40,41]. Studies are underway to understand the effect of combining immunotherapy with HDRT on these TAMs and asses their role in tumor growth inhibition in our model. We also plan to extend the utilization of 9464D tumor model by investigating the effect of combining HDRT with other immunotherapeutic approaches.

In an era of targeted immunotherapy, the development of a novel syngeneic mice model is important for preclinical investigation for high risk neuroblastoma as it allow us to test cancer therapies in the presence of a functional immune system. Here we developed one such model and showed that it is an effective tool to use for the development of novel multimodal therapies for neuroblastoma.

Declarations

Author contribution statement

Shuobo Boboila: Conceived and designed the experiments; Performed the experiments; Analyzed and interpreted the data; Contributed reagents, materials, analysis tools or data.

Shunpei Okochi: Conceived and designed the experiments; Performed the experiments; Analyzed and interpreted the data; Wrote the paper.

Debarshi Banerjee: Performed the experiments; Analyzed and interpreted the data; Contributed reagents, materials, analysis tools or data; Wrote the paper.

Sunjay Barton; Cherease Street: Performed the experiments; Contributed reagents, materials, analysis tools or data.

Ariela L Zenilman; Qi Wang: Analyzed and interpreted the data; Contributed reagents, materials, analysis tools or data.

Robyn D. Gartrell; Yvonne M. Saenger; David Welch; Cheng-Chia Wu; Angela Kadenhe-Chiweshe: Contributed reagents, materials, analysis tools or data.

Darrell J. Yamashiro; Eileen P. Connolly: Conceived and designed the experiments; Analyzed and interpreted the data.

Data availability statement

Data included in article/supplementary material/referenced in article.

Funding statement

This research was funded in part through the NIH/NCI Cancer Center Support Grant P30CA013696, NIH Shared Instrument Grant

S10-OD010631-01A1, Pediatric Cancer Foundation (DJY), Young Investigator Award from Alex's Lemonade Stand Foundation (SB), tay-bandz foundation (DJY), Swim Across America (RDG), NIH TL1 Grant 1TL1TR001875-01 (RDG).

Declaration of competing interest

The authors declare that they have no known competing financial interests or personal relationships that could have appeared to influence the work reported in this paper.

Appendix A. Supplementary data

Supplementary data to this article can be found online at https://doi.org/10.1016/j.heliyon.2023.e17399.

References

[1] K.K. Matthay, R.E. George, A.L. Yu, Promising therapeutic targets in neuroblastoma, Clin. Cancer Res. : Off. J. Am. Ass. Canc. Res. 18 (10) (2012) 2740–2753.
[2] S.E. Rha, J.Y. Byun, S.E. Jung, H.J. Chun, H.G. Lee, J.M. Lee, Neurogenic tumors in the abdomen: tumor types and imaging characteristics, Radiographics : Rev. Pub. Radiolog. Soci. North Am. Inc. 23 (1) (2003) 29–43.
[3] N.K. Cheung, M.A. Dyer, Neuroblastoma: developmental biology, cancer genomics and immunotherapy, Nat. Rev. Cancer 13 (6) (2013) 397–411.
[4] A. Arina, S.I. Gutiontov, R.R. Weichselbaum, Radiotherapy and Immunotherapy for Cancer: from "systemic" to "Multi-Site, Clinical cancer research : an official journal of the American Association for Cancer Research, 2020.
[5] M. Spiotto, Y.X. Fu, R.R. Weichselbaum, The intersection of radiotherapy and immunotherapy: mechanisms and clinical implications, Sci. Immunol. 1 (3) (2016).
[6] R.R. Weichselbaum, H. Liang, L. Deng, Y.X. Fu, Radiotherapy and immunotherapy: a beneficial liaison? Nat. Rev. Clin. Oncol. 14 (6) (2017) 365–379.
[7] L.C. Brown, R.A. Lester, M.P. Grams, M.G. Haddock, K.R. Olivier, C.A. Arndt, et al., Stereotactic body radiotherapy for metastatic and recurrent ewing sarcoma and osteosarcoma, Sarcoma 2014 (2014), 418270.
[8] J. Deck, G. Eastwick, J. Sima, A. Raymond, J. Bogart, P. Aridgides, Efficacy and tolerability of stereotactic body radiotherapy for lung metastases in three patients with pediatric malignancies, OncoTargets Ther. 12 (2019) 3723–3727.
[9] B. Farnia, C.U. Louis, B.S. Teh, A.C. Paulino, Stereotactic body radiation therapy (SBRT) for an isolated bone metastasis in an adolescent male with nasopharyngeal carcinoma, Pediatr. Blood Cancer 61 (8) (2014) 1520.
[10] N.K. Taunk, B. Kushner, K. Ibanez, S.L. Wolden, Short-interval retreatment with stereotactic body radiotherapy (SBRT) for pediatric neuroblastoma resulting in severe myositis, Pediatr. Blood Cancer 63 (4) (2016) 731–733.
[11] A.P. Dove, B.A. Manole, D.V. Wakefield, S.J. Cross, M. Doubrovin, B.L. Shulkin, et al., Managing local-regional failure in children with high-risk neuroblastoma: a single institution experience, Pediatr. Blood Cancer 65 (12) (2018), e27408.
[12] H.N. Lode, R. Xiang, N.M. Varki, C.S. Dolman, S.D. Gillies, R.A. Reisfeld, Targeted interleukin-2 therapy for spontaneous neuroblastoma metastases to bone marrow, J. Natl. Cancer Inst. 89 (21) (1997) 1586–1594.
[13] A. Wierzbicki, M. Gil, M. Ciesielski, R.A. Fenstermaker, Y. Kaneko, H. Rokita, et al., Immunization with a mimotope of GD2 ganglioside induces CD8+ T cells that recognize cell adhesion molecules on tumor cells, J. Immunol. 181 (9) (2008) 6644–6653.
[14] W.A. Weiss, K. Aldape, G. Mohapatra, B.G. Feuerstein, J.M. Bishop, Targeted expression of MYCN causes neuroblastoma in transgenic mice, EMBO J. 16 (11) (1997) 2985–2995.
[15] A. Beckers, G. Van Peer, D.R. Carter, M. Gartlgruber, C. Herrmann, S. Agarwal, et al., MYCN-driven regulatory mechanisms controlling LIN28B in neuroblastoma, Canc. Letter. 366 (1) (2015) 123–132.
[16] T. Teitz, J.J. Stanke, S. Federico, C.L. Bradley, R. Brennan, J. Zhang, et al., Preclinical models for neuroblastoma: establishing a baseline for treatment, PLoS One 6 (4) (2011), e19133.
[17] C.M. Moran, S.D. Pye, W. Ellis, A. Janeczko, K.D. Morris, A.S. McNeilly, et al., A comparison of the imaging performance of high resolution ultrasound scanners for preclinical imaging, Ultrasound Med. Biol. 37 (3) (2011) 493–501.
[18] J. Duraiswamy, K.M. Kaluza, G.J. Freeman, G. Coukos, Dual blockade of PD-1 and CTLA-4 combined with tumor vaccine effectively restores T-cell rejection function in tumors, Cancer Res. 73 (12) (2013) 3591–3603.
[19] S. Koyama, E.A. Akbay, Y.Y. Li, G.S. Herter-Sprie, K.A. Buczkowski, W.G. Richards, et al., Adaptive resistance to therapeutic PD-1 blockade is associated with upregulation of alternative immune checkpoints, Nat. Commun. 7 (2016), 10501.
[20] W. Wang, J.M. Marinis, A.M. Beal, S. Savadkar, Y. Wu, M. Khan, et al., RIP1 kinase drives macrophage-mediated adaptive immune tolerance in pancreatic cancer, Cancer Cell 34 (5) (2018) 757–774 e7.
[21] D. Welch, A.D. Harken, G. Randers-Pehrson, D.J. Brenner, Construction of mouse phantoms from segmented CT scan data for radiation dosimetry studies, Phys. Med. Biol. 60 (9) (2015) 3589–3598.
[22] D. Welch, L. Turner, M. Speiser, G. Randers-Pehrson, D.J. Brenner, Scattered dose calculations and measurements in a life-like mouse phantom, Radiat. Res. 187 (4) (2017) 433–442.
[23] D. Banerjee, S.M. Barton, P.W. Grabham, A.L. Rumeld, S. Okochi, C. Street, et al., High-Dose Radiation increases Notch1 in tumor vasculature, Int. J. Radiat. Oncol. Biol. Phys.106(4) (2019) 857–866.
[24] G. Papaioannou, K. McHugh, Neuroblastoma in childhood: review and radiological findings, Cancer Imag. : Off. Pub. Int. Canc. Imag. Soci. 5 (2005) 116–127.
[25] A.E. Albregts, M.D. Cohen, C.A. Galliani, Neuroblastoma invading the kidney, J. Pediatr. Surg. 29 (7) (1994) 930–933.
[26] Lim II, D.A. Goldman, B.A. Farber, J.M. Murphy, S.J. Abramson, E. Basu, et al., Image-defined risk factors for nephrectomy in patients undergoing neuroblastoma resection, J. Pediatr. Surg. 51 (6) (2016) 975–980.
[27] H. Deng, C.W. Kennedy, E. Armour, E. Tryggestad, E. Ford, T. McNutt, et al., The small-animal radiation research platform (SARRP): dosimetry of a focused lens system, Phys. Med. Biol. 52 (10) (2007) 2729–2740.
[28] S.J. Dovedi, E.J. Cheadle, A.L. Popple, E. Poon, M. Morrow, R. Stewart, et al., Fractionated radiation therapy stimulates antitumor immunity mediated by both resident and infiltrating polyclonal T-cell populations when combined with PD-1 blockade, Clin. Cancer Res. : Off. J. Am. Ass. Canc. Res. 23 (18) (2017) 5514–5526.
[29] J. Gong, T.Q. Le, E. Massarelli, A.E. Hendifar, R. Tuli, Radiation therapy and PD-1/PD-L1 blockade: the clinical development of an evolving anticancer combination, J. Immunother. Canc. 6 (1) (2018) 46.
[30] A. Dondero, F. Pastorino, M. Della Chiesa, M.V. Corrias, F. Morandi, V. Pistoia, et al., PD-L1 expression in metastatic neuroblastoma as an additional mechanism for limiting immune surveillance, OncoImmunology 5 (1) (2016), e1064578.
[31] C.L. Tinkle, C. Singh, S. Lloyd, Y. Guo, Y. Li, A.S. Pappo, et al., Stereotactic body radiation therapy for metastatic and recurrent solid tumors in children and young adults, Int. J. Radiat. Oncol. Biol. Phys. 109 (5) (2021) 1396–1405.

[32] R.D. Gartrell, D.K. Marks, T.D. Hart, G. Li, D.R. Davari, A. Wu, et al., Quantitative analysis of immune infiltrates in primary melanoma, Canc. Immun. Res. 6 (4) (2018) 481–493.
[33] J. Nolan, T. Frawley, J. Tighe, H. Soh, C. Curtin, O. Piskareva, Preclinical models for neuroblastoma: advances and challenges, Canc. Letter. 474 (2020) 53–62.
[34] A. Kamili, C. Atkinson, T.N. Trahair, J.I. Fletcher, Mouse models of high-risk neuroblastoma, Cancer Metastasis Rev. 39 (1) (2020) 261–274.
[35] M. Pelleitier, S. Montplaisir, The nude mouse: a model of deficient T-cell function, Methods Achiev. Exp. Pathol. 7 (1975) 149–166.
[36] D.M. Patterson, J.M. Shohet, E.S. Kim, Preclinical models of pediatric solid tumors (neuroblastoma) and their use in drug discovery, Curr. Protoc. Pharmacol.52 (1) (2011) 14–17.
[37] D. Banerjee, S.L. Hernandez, A. Garcia, T. Kangsamaksin, E. Sbiroli, J. Andrews, et al., Notch suppresses angiogenesis and progression of hepatic metastases, Cancer Res. 75 (8) (2015) 1592–1602.
[38] J. Huang, J.S. Frischer, A. Serur, A. Kadenhe, A. Yokoi, K.W. McCrudden, et al., Regression of established tumors and metastases by potent vascular endothelial growth factor blockade, Proc. Natl. Acad. Sci. U. S. A 100 (13) (2003) 7785–7790.
[39] O. Tavana, D. Li, C. Dai, G. Lopez, D. Banerjee, N. Kon, et al., HAUSP deubiquitinates and stabilizes N-Myc in neuroblastoma, Nat. Med. 22 (10) (2016) 1180–1186.
[40] X. Shi, S.L. Shiao, The role of macrophage phenotype in regulating the response to radiation therapy, Transl. Res. 191 (2018) 64–80.
[41] C. Beach, D. MacLean, D. Majorova, J.N. Arnold, M.M. Olcina, The effects of radiation therapy on the macrophage response in cancer, Front. Oncol. (2022).